Calculation of BR($\bar{B}^0 \to \Lambda_c^+ + \bar{p}$) in the perturbative QCD approach

Xiao-Gang He,[1,2] Tong Li,[1] Xue-Qian Li,[1] and Yu-Ming Wang[1]
[1]*Department of Physics, Nankai University, Tianjin*
[2]*Department of Physics and Center for Theoretical Sciences, National Taiwan University, Taipei*
(Received 25 October 2006; published 22 February 2007)

We calculate the branching ratio of $\bar{B}^0 \to \Lambda_c^+ \bar{p}$ in the PQCD approach. Most previous model calculations obtained branching ratios significantly larger than experimental data. We find that the predicted branching ratio for BR($\bar{B}^0 \to \Lambda_c^+ \bar{p}$) in the PQCD approach can vary over a range of $(2.3 \sim 5.1) \times 10^{-5}$ with the largest uncertainty coming from the parameters in the wave function of Λ_c. With the favored values for the parameters in the Λ_c^+ wave function, $\beta = 1$ GeV and $m_q = 0.3$ GeV, the branching ratio is about 2.3×10^{-5} which is satisfactorily consistent with the value measured by experiments.

DOI: 10.1103/PhysRevD.75.034011 PACS numbers: 13.25.Hw, 12.38.Bx

I. INTRODUCTION

B-physics stands as an ideal laboratory for studying hadron structure and fundamental mechanisms which govern the reactions for a heavy quark and the related hadronization processes. It also offers a window to search for new physics. The mesonic decays of *B* meson have been carefully studied already by many authors because such processes are theoretically simpler and have a rich data accumulation. Nevertheless, much data on the baryonic decays of *B* mesons also have been collected. In 1987, $B \to p\bar{p}\pi^{\pm}$ and $B \to p\bar{p}\pi^+\pi^-$ were first observed by ARGUS [1] and since then, various baryonic-decay modes of *B* meson were measured at CLEO, Belle, and *BABAR* [2–6]. All the information offers us an opportunity to more seriously investigate the processes where baryons are involved. However, the case for baryonic decays is much more complicated than the mesonic one, especially in the perturbative QCD (PQCD) approach [7] where there is no any real spectator constituent, namely, all the constituents must be connected by gluons. One also needs to have detailed information about the wave functions of baryons which contain three valence quarks. All these make the problem much more complicated and cause theoretical uncertainties.

In this work we study the process $\bar{B}^0 \to \Lambda_c^+ \bar{p}$. This process has been measured [3–5] with a branching ratio of [6] $(2.2 \pm 0.8) \times 10^{-5}$. There have been some theoretical evaluations for this branching ratio using various phenomenological models, such as the constituent quark model, the pole model, the QCD sum rule, the diquark model, and others [8–12]. All the theoretical predictions made in these models are substantially larger than the data. Later Cheng and Yang [13] considered the pole structure and applied the bag model for calculating the hadronic matrix element. Their result is close to the experimental data. The related theoretical estimations on the branching ratio and the experimental data are listed in Table I.

The wide range of predicted branching ratio for $\bar{B}^0 \to \Lambda_c^+ \bar{p}$ indicates that at present theoretical understanding is not satisfactory. A way to distinguish different methods may be systematically using the same method to evaluate several different branching ratios. Our emphasis in this work is to establish PQCD calculation for $\bar{B} \to \Lambda_c^+ \bar{p}$. There is always the question of how reliable PQCD calculation is and what is the soft contribution which is not included in the PQCD calculation. Without a coherent method being able to handle perturbative and nonperturbative effects, it is not possible to properly address this problem and we will not attempt to do it here either. Our choice of PQCD framework is encouraged by successful application to mesonic *B* decays. Therefore, our aim is to establish a PQCD calculation for $\bar{B}^0 \to \Lambda_c^+ \bar{p}$ and obtain the branching ratio.

Since the success of the PQCD approach in studying mesonic decays of *B* meson is remarkable, it is natural to extend this approach to evaluate the decay rates of baryonic decays of *B* mesons. In $\bar{B}^0 \to \Lambda_c^+ \bar{p}$, the two final baryons are much lighter than *B* meson, they possess relatively large linear-momentum $\mathbf{p} = \lambda^{1/2}(M_B^2, M_{\Lambda_c}^2, M_p^2)/2M_B$ in the rest frame of *B* meson, thus the momentum match of the quarks in the final baryons requires that the exchanged gluons must be ''hard,'' or say, have large k^2. Here k indicates the generic momentum carried by a gluon. Moreover, unlike in some cases where a pair of quark-antiquark is created from vacuum, the pair of quark-antiquark is created by a hard gluon; therefore, one expects that the whole process is calculable in the framework of PQCD [14].

In the PQCD approach, there are unknown parameters in the wave functions of the *B* meson and the two baryons in the final state. However, since these parameters are universal, they can be fixed by fitting data of other relevant decays. This treatment on the unknown parameters reduces the model dependence of the theoretical calculations. Therefore, one has good reasons to believe that the result obtained in PQCD would be credible. Indeed, our numerical result is closer to the experimental data than those by other models.

The effective Hamiltonian responsible at the quark level for $\bar{B}^0 \to \Lambda_c^+ \bar{p}$ is given by [15]

TABLE I. Branching ratio of $\bar{B}^0 \to \Lambda_c^+ \bar{p}$ obtained with different models and experiments (last two numbers), respectively. There is also a preliminary *BABAR* result [4] $(2.15 \pm 0.36 \pm 0.13 \pm 0.56) \times 10^{-5}$.

$\bar{B}^0 \to \Lambda_c^+ \bar{p}$	[9]	[10]	[11]	[12]	[13]	[3]	[5]
BR	4×10^{-4}	8.5×10^{-4}	1.1×10^{-3}	$(1.7 \sim 1.9) \times 10^{-3}$	1.1×10^{-5}	$(2.19^{+0.56}_{-0.49} \pm 0.32 \pm 0.57) \times 10^{-5}$	$<9 \times 10^{-5}$

$$H_{\rm eff} = \frac{G_F}{\sqrt{2}} V_{cb} V_{ud}^* [C_1 (\bar{c}b)_{V-A} (\bar{d}u)_{V-A} + C_2 (\bar{c}u)_{V-A} \times (\bar{d}b)_{V-A}] + \text{H.c.}, \quad (1)$$

where $(\bar{a}b)_{V-A} = \bar{a}\gamma^\mu(1-\gamma_5)b$, and $C_1^{\rm LO}(m_b) = 1.12$, $C_2^{\rm LO}(m_b) = -0.27$ [15]. In our calculation the μ dependence of $C_{1,2}$ at the leading order remains.

At the hadron level, the decay amplitude for $\bar{B}^0 \to \Lambda_c^+ \bar{p}$ is obtained by sandwiching the effective Hamiltonian between the initial and final hadron states,

$$M(\bar{B}^0 \to \Lambda_c^+ \bar{p}) = \langle \Lambda_c^+ \bar{p} | H_{\rm eff} | \bar{B}^0 \rangle = \frac{G_F}{\sqrt{2}} V_{cb} V_{ud}^* \bar{\Lambda}_c^+ (A + B\gamma_5) p, \quad (2)$$

where A and B are two form factors which we will calculate in the PQCD approach.

The partial decay width is then given by

$$\Gamma(\bar{B}^0 \to \Lambda_c^+ \bar{P}) = \frac{G_F^2 |V_{cb}|^2 |V_{ud}|^2}{16 m_B^3 \pi} \times \sqrt{(m_B^2 - (m_{\Lambda_c} + m_P)^2)(m_B^2 - (m_{\Lambda_c} - m_P)^2)} \times [|A|^2 (m_B^2 - (m_{\Lambda_c} + m_P)^2) + |B|^2 (m_B^2 - (m_{\Lambda_c} - m_P)^2)]. \quad (3)$$

In the following sections we present details for the calculations. In Sec. II we describe the approach for calculations. In Sec. III we present our numerical results along with all necessary input parameters. The last section is devoted to our discussions and conclusions. Some details for calculations of the diagrams are given in the appendices.

II. PQCD CALCULATION OF THE HADRONIC MATRIX ELEMENTS

The effective Hamiltonian at quark level has been studied by many authors and the PQCD approach also has been discussed extensively in literature. In this section we discuss how to calculate the hadronic matrix elements defined in the previous section in terms of the PQCD method [7,16–18]. As usual, we define, in the rest frame of $\bar{B}^0$, q, p, and p' to be the four-momenta of $\bar{B}^0$, Λ_c^+ and antiproton, $q_i (i = 1, 2)$, k_i, and $k_i' (i = 1, 2, 3)$ to be the momenta of the valance light quarks (antiquark) inside $\bar{B}^0$, Λ_c^+, and $\bar{p}$, respectively. We parameterize the corresponding light-cone momenta with the masses of all light quarks and antiproton being neglected as

$$\begin{aligned} q &= (q^+, q^-, \mathbf{0}_T) = \frac{m_B}{\sqrt{2}}(1, 1, \mathbf{0}_T), \\ p &= (p^+, p^-, \mathbf{0}_T) = (q^+, r^2 q^-, \mathbf{0}_T) = \frac{m_B}{\sqrt{2}}(1, r^2, \mathbf{0}_T) \\ p' &= (0, p'^-, \mathbf{0}_T) = \frac{m_B}{\sqrt{2}}(0, 1 - r^2, \mathbf{0}_T) \\ q_1^{(1)} &= (y q^+, q^-, \mathbf{q}_T), \qquad q_2^{(1)} = ((1-y) q^+, 0, -\mathbf{q}_T) \quad (4) \\ k_1 &= (x_1 p^+, p^-, \mathbf{k}_{1T}), \qquad k_2 = (x_2 p^+, 0, \mathbf{k}_{2T}), \\ k_3 &= (x_3 p^+, 0, \mathbf{k}_{3T}) \qquad k_1' = (0, x_1' p'^-, \mathbf{k}_{1T}'), \\ k_2' &= (0, x_2' p'^-, \mathbf{k}_{2T}'), \qquad k_3' = (0, x_3' p'^-, \mathbf{k}_{3T}'), \end{aligned}$$

where $r = m_{\Lambda_c}/m_B$, and y, x_i, x_i' are the fractions of the longitudinal momenta of the valence quarks with $x_1 + x_2 + x_3 = 1$ and $x_1' + x_2' + x_3' = 1$. $\mathbf{q}_T$, $\mathbf{k}_{iT}$, and $\mathbf{k}_{iT}'$ are the transverse momenta of the valence quarks inside $\bar{B}^0$, Λ_c^+ and antiproton, respectively.

Note that because $\bar{B}^0$ is in its rest frame, even though the momenta of the valance quarks inside the final states $(\Lambda_c^+, \bar{p})$ are fixed, the four-momenta of the valance quarks inside $\bar{B}^0$ (q_1, q_2) are not uniquely determined. Generally, there are two distinct cases. Besides the above assignment of the momenta, one may also set

$$q_1^{(2)} = (q^+, y q^-, \mathbf{q}_T), \qquad q_2^{(2)} = (0, (1-y) q^-, -\mathbf{q}_T). \quad (5)$$

The first case $(q_i^{(1)})$ corresponds to that the momenta of $\bar{d}$-quarks in initial state $\bar{B}^0$ and final state $\bar{p}$ are opposite to each other, and the second one $(q_i^{(2)})$ is that they are parallel. The two cases contribute to different Feynaman diagrams according to the general rule of PQCD (see the figures below for details), thus one needs to make careful analysis to determine which case is the correct choice when convoluting the initial light-cone wave function with the final light-cone wave functions.

In the PQCD picture, hadrons are made of valence quarks whose momenta distributions are described by appropriate wave functions. The wave function of Λ_c is usually defined through the correlator [19],

$$(Y_{\Lambda_c})_{\alpha\beta\gamma}(k_i,\nu) = \frac{1}{2\sqrt{2}N_c}\int\prod_{l=2}^{3}\frac{dw_l^+ d\mathbf{w_l}}{(2\pi)^3}e^{ik_l w_l}\varepsilon^{abc} \times\langle 0|T[c_\alpha^a(0)u_\beta^b(w_2)d_\gamma^c(w_3)]|\Lambda_c(p)\rangle = \frac{f_{\Lambda_c}}{8\sqrt{2}N_c}[(\not{p}+m_{\Lambda_c})\gamma_5 C]_{\beta\gamma}[\Lambda_c(p)]_\alpha \times\Psi(k_i,\nu), \quad (6)$$

where f_{Λ_c} is a normalization constant, $\Lambda_c(p)$ is the Λ_c spinor, and $\Psi(k_i,\nu)$ is its wave function. ν is the hard subamplitude energy scale for the process which is within the range of $\Lambda_{\rm QCD} < \nu < m_b$ and will be further discussed below. Similarly, the leading-twist wave function of proton is defined by [16,20]

$$(Y_P)_{\alpha\beta\gamma}(k_i',\nu) = \frac{1}{2\sqrt{2}N_c}\int\prod_{l=1}^{2}\frac{dw_l^- d\mathbf{w_l}}{(2\pi)^3}e^{ik_l' w_l}\varepsilon^{abc} \times\langle 0|T[u_\alpha^a(w_1)u_\beta^b(w_2)d_\gamma^c(0)]|P(p')\rangle = \frac{f_P(\nu)}{8\sqrt{2}N_c}\{(\not{p}'C)_{\beta\gamma}[\gamma_5 P(p')]_\alpha\Phi^V(k_i',\nu) + (\not{p}'\gamma_5 C)_{\beta\gamma}[P(p')]_\alpha\Phi^A(k_i',\nu) - (\sigma_{\mu\nu}p'^\nu C)_{\beta\gamma}[\gamma^\mu\gamma_5 P(p')]_\alpha\Phi^T(k_i',\nu)\}, \quad (7)$$

where f_P is the normalization constant, and $P(p')$ is the proton spinor,

$$\Phi^V(k_1',k_2',k_3',\nu) = \tfrac{1}{2}[\Phi(k_2',k_1',k_3',\nu)+\Phi(k_1',k_2',k_3',\nu)],$$
$$\Phi^A(k_1',k_2',k_3',\nu) = \tfrac{1}{2}[\Phi(k_2',k_1',k_3',\nu)-\Phi(k_1',k_2',k_3',\nu)],$$
$$\Phi^T(k_1',k_2',k_3',\nu) = \tfrac{1}{2}[\Phi(k_1',k_3',k_2',\nu)+\Phi(k_2',k_3',k_1',\nu)]. \quad (8)$$

The B meson wave function is expressed as [21]

$$(Y_B)_{\alpha\beta}(q_i,\nu) = \frac{1}{N_c}\int\frac{d^4w}{(2\pi)^4}e^{iq_2\cdot w}\langle 0|T[\bar{d}_\alpha(w)b_\beta(0)]|\bar{B}^0(q)\rangle = \frac{i}{\sqrt{2N_c}}\left[(\not{q}+m_B)\gamma_5\left(\frac{\not{n}_+}{\sqrt{2}}\phi_B^+(q_2,\nu) + \frac{\not{n}_-}{\sqrt{2}}\phi_B^-(q_2,\nu)\right)\right]_{\beta\alpha}. \quad (9)$$

where $\not{n}_+$ term corresponds to the first choice of momenta of the valance quark $\bar{d}$ in $\bar{B}^0$, and $\not{n}_-$ term corresponds to the second one with the relation

$$\frac{\not{n}_\pm}{\sqrt{2}} = \frac{\not{q}_2^{1,2}}{(1-y)m_B}. \quad (10)$$

When convoluting the hadron wave functions with the hard amplitude, one should use corresponding light-cone momenta $q_i^{1,2}$ consistently for the above two terms.

There is also a simple relation between wave functions ϕ_B^+, ϕ_B^- and ϕ_B, $\bar{\phi}_B$ used in the usual PQCD calculation:

$$\phi_B^+ = \phi_B + \bar{\phi}_B, \qquad \phi_B^- = \phi_B - \bar{\phi}_B. \quad (11)$$

It has been argued that the distribution amplitude $\bar{\phi}_B$ is negligible compared to ϕ_B [21]; therefore, $\phi_B^+ = \phi_B^- \simeq \phi_B$. The specific form of ϕ_B will be given later when carrying out numerical calculations.

Including the Sudakov factor with infrared cutoffs $\omega(\omega',\omega_q)$, and running the wave function from ν down to $\omega(\omega',\omega_q)$, the wave functions are obtained as [16]

$$\Psi(x_i,b_i,p,\nu) = \exp\left[-\sum_{l=2}^{3}s(\omega,x_l p^+) - 3\int_\omega^\nu\frac{d\bar{\mu}}{\bar{\mu}}\gamma_q(\alpha_s(\bar{\mu}))\right]\Psi(x_i)$$
$$\Phi(x_i',b_i',p',\nu) = \exp\left[-\sum_{l=1}^{3}s(\omega',x_l' p^-) - 3\int_{\omega'}^\nu\frac{d\bar{\mu}}{\bar{\mu}}\gamma_q(\alpha_s(\bar{\mu}))\right]\Phi(x_i',\omega'),$$
$$\Phi_B(y,b_q,q,\nu) = \exp\left[-s(\omega_q,q_2^+) - 2\int_{\omega_q}^\nu\frac{d\bar{\mu}}{\bar{\mu}}\gamma(\alpha_s(\bar{\mu}))\right]\Phi_B(1-y), \quad (12)$$

where $\omega = \min(1/\tilde{b}_1, 1/\tilde{b}_2, 1/\tilde{b}_3)$, $\omega' = \min(1/\tilde{b}_1', 1/\tilde{b}_2', 1/\tilde{b}_3')$, and $\omega_q = 1/b_q$. $\tilde{b}_1^{(\prime)} = |\mathbf{b}_2^{(\prime)} - \mathbf{b}_3^{(\prime)}|$, $\tilde{b}_2^{(\prime)} = |\mathbf{b}_1^{(\prime)} - \mathbf{b}_3^{(\prime)}|$, $\tilde{b}_3^{(\prime)} = |\mathbf{b}_1^{(\prime)} - \mathbf{b}_2^{(\prime)}|$, and $b_q = |\mathbf{b}_q|$. Here $\mathbf{b}$, $\mathbf{b}'$, and $\mathbf{b}_q$ are the conjugate variables to $\mathbf{k}_T$, $\mathbf{k}_T'$, and $\mathbf{q}_T$ whose definitions are collected in Appendix D.

The explicit expressions for the Sudakov factors are given in [16] with

$$s(\omega,Q) = \int_\omega^Q\frac{dp}{p}\left[\ln\left(\frac{Q}{p}\right)A[\alpha_s(p)] + B[\alpha_s(p)]\right],$$
$$A = C_F\frac{\alpha_s}{\pi} + \left[\frac{67}{9} - \frac{\pi^2}{3} - \frac{10}{27}n_f + \frac{8}{3}\beta_0\ln\left(\frac{e^{\gamma_E}}{2}\right)\right]\left(\frac{\alpha_s}{\pi}\right)^2,$$
$$B = \frac{2}{3}\frac{\alpha_s}{\pi}\ln\left(\frac{e^{2\gamma_E-1}}{2}\right), \qquad \gamma_q(\alpha_s(\mu)) = -\alpha_s(\mu)/\pi,$$
$$\beta_0 = \frac{33-2n_f}{12}, \quad (13)$$

where γ_E is the Euler constant, n_f is the flavor number, and γ_q is the anomalous dimension. For B decays, the typical energy scale is above the charm mass, so we will take n_f to be 4 in our numerical computations.

Within the PQCD framework, the hadronic matrix element can be written as

$$M = \int [Dx] \int [Db] (\bar{Y}_{\Lambda_c})_{\alpha'\beta'\gamma'}(x_i', b_i', p', \nu) \times H^{\alpha'\beta'\gamma'\rho'\alpha\beta\gamma\rho}(x_i, x_i', y, b_i, b_i', b_q, m_B, m_{\Lambda_c}, \nu) \times (Y_{\bar{p}})_{\alpha\beta\gamma}(x_i, b_i, p, \nu)(Y_B)_{\rho\rho'}(y, b_q, q, \nu), \quad (14)$$

where

$$[Dx] = [dx][dx']dy,$$
$$[dx] = dx_1 dx_2 dx_3 \delta\Big(1 - \sum_{l=1}^{3} x_l\Big), \quad (15)$$
$$[dx'] = dx_1' dx_2' dx_3' \delta\Big(1 - \sum_{l=1}^{3} x_l'\Big).$$

The measures of the transverse parts $[Db]$ are defined in Appendix A for several examples.

To obtain the hard scattering amplitude $H^{\alpha'\beta'\gamma'\rho'\alpha\beta\gamma\rho}(x, x', y, b, b', b_q, m_B, m_{\Lambda_c}, \nu)$, one first derives the amplitude $H^{i,\alpha'\beta'\gamma'\rho'\alpha\beta\gamma\rho}(x_i, x_i', y, \mathbf{k}_T, \mathbf{k}_T', \mathbf{q}_T, m_B, m_{\Lambda_c})$ corresponding to the ith diagram in Figs. 1–3. Some sample analytic expressions are displayed in Appendix B. Then a Fourier transformation on $\mathbf{k}_T$ and $\mathbf{k}_T'$ is carried out to convert them into the $\mathbf{b}$ and $\mathbf{b}'$ space to obtain $\tilde{H}^{i,\alpha'\beta'\gamma'\rho'\alpha\beta\gamma\rho}(x, x', y, b, b', b_q, m_B, m_{\Lambda_c})$. The concrete procedure for such transformation is described at the end of Appendix D.

We can catalog the diagrams into several types. The first type includes 36 diagrams, indicated by a_i in Fig. 1. If we adopt the first choice of momenta (q_i^1) of valance quark in $\bar{B}^0$ the total 36 diagrams contribute to the amplitude in the PQCD frame, where the gluons can be "hard" (have large k^2). However, one can notice that, if we adopt the second choice (q_i^2), in some of the diagrams the gluon attached to the spectator quark is always soft, i.e. $k^2 \approx 0$. The contributions of such diagrams cannot be counted as PQCD contributions and are attributed into the wave functions of the initial or final hadrons. When calculating the PQCD contributions, these diagrams should not be included at all. In that case, only 8 diagrams, indicated by b_i in Fig. 2 remain where all the exchanged gluons are hard. For another type of diagrams, indicated by c_i in Fig. 3, three-gluon vertices are involved. We find that the color factor for two, $c_{3,4}$, of them is zero. There are also the W exchange diagrams (where W is exchanged between the initial b and $\bar{d}$). In 36 of them gluons are only connected to quark lines, whereas in the other 4 of them three-gluon vertices are involved, as shown in Fig. 4. These diagrams are suppressed by the linear-momentum match and usually ignored [13]. Therefore, there are $36 + 8 + 2 = 46$ diagrams shown in Figs. 1–3, that need to be evaluated to the leading order.

Multiplying all contributions of the diagrams in Figs. 1–3 with corresponding Wilson coefficients, one adds them up to obtain the full hard scattering amplitude

$$H^{\alpha'\beta'\gamma'\rho'\alpha\beta\gamma\rho}(x, x', y, b, b', b_q, m_B, m_{\Lambda_c}) = \sum_i C(t) \tilde{H}^{i,\alpha'\beta'\gamma'\rho'\alpha\beta\gamma\rho}(x, x', y, b, b', b_q, m_B, m_{\Lambda_c}).$$

Here we denote the hard scale as t which is taken to be the larger of the two variables $t_{1,2}$ associated with the virtual gluon momentum in Fig. 1, i.e. $t = \max(t_1^i, t_2^i)$. The expressions for $t_{1,2}$ are listed in Appendix C.

Finally, a renormalization group running is applied to the hard scattering amplitude from the scale ν in the wave functions to t, and we obtain

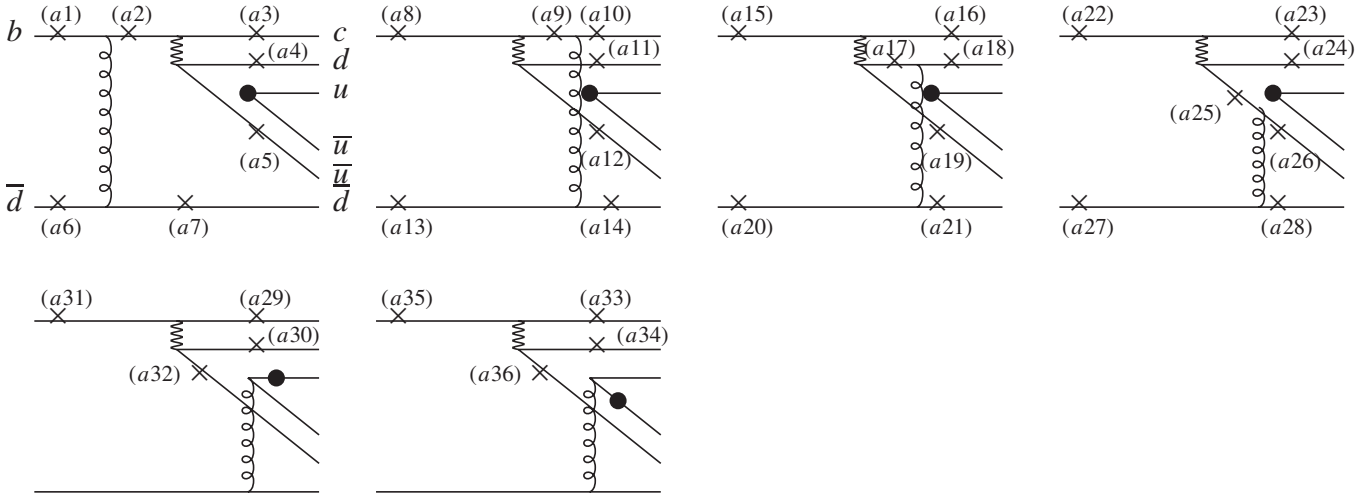

FIG. 1. The lowest order diagrams for the $\bar{B}^0 \to \Lambda_c^+ \bar{p}$ decay according to the first choice of momenta (q_i^1). The wavy line indicates W exchange. The solid lines and curly lines denote the quarks and gluons, respectively. In the diagrams, only one gluon line is shown. The other gluon line connects the solid black blob and the cross indicated by a_i. There are 36 diagrams. We label each one by a_i.

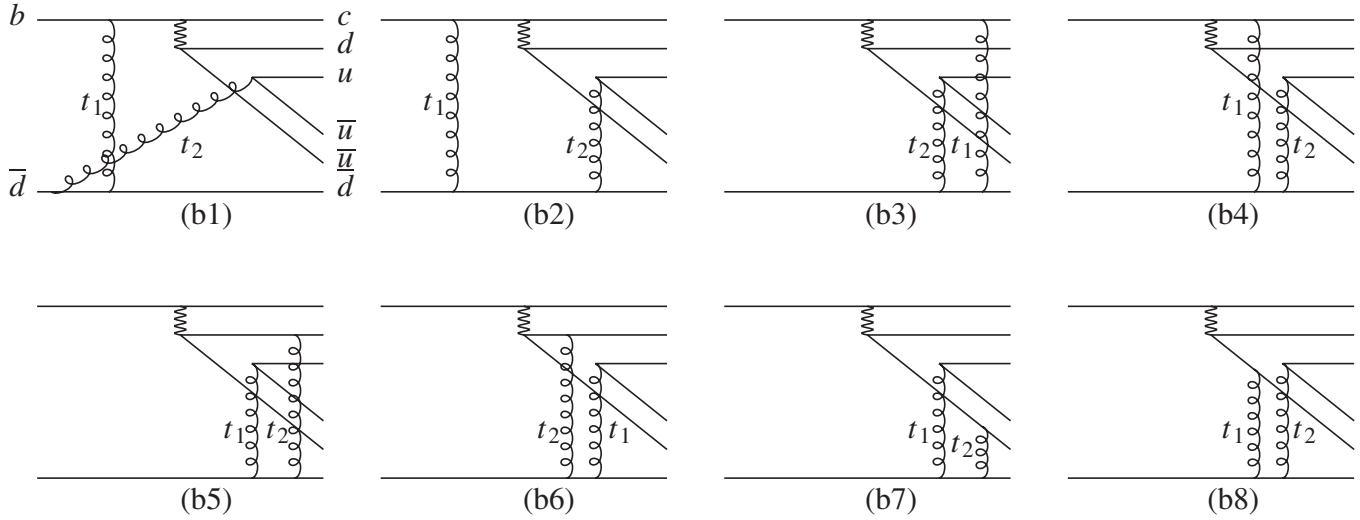

FIG. 2. The lowest order diagrams for the $\bar{B}^0 \to \Lambda_c^+ \bar{p}$ decay according to the second choice of momenta (q_i^2). The wavy line indicates W exchange. The solid lines and curly lines denote the quarks and gluons, respectively. There are 8 diagrams. We label each one by b_i.

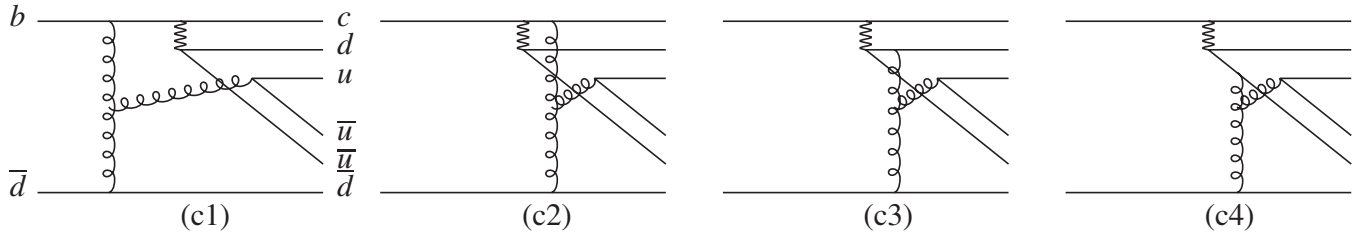

FIG. 3. The lowest order diagrams for the $\bar{B}^0 \to \Lambda_c^+ \bar{p}$ decay including three-gluon vertices. The wavy line indicates W exchange. The solid lines and curly lines denote the quarks and gluons, respectively. There are 4 diagrams. We label each one by c_i.

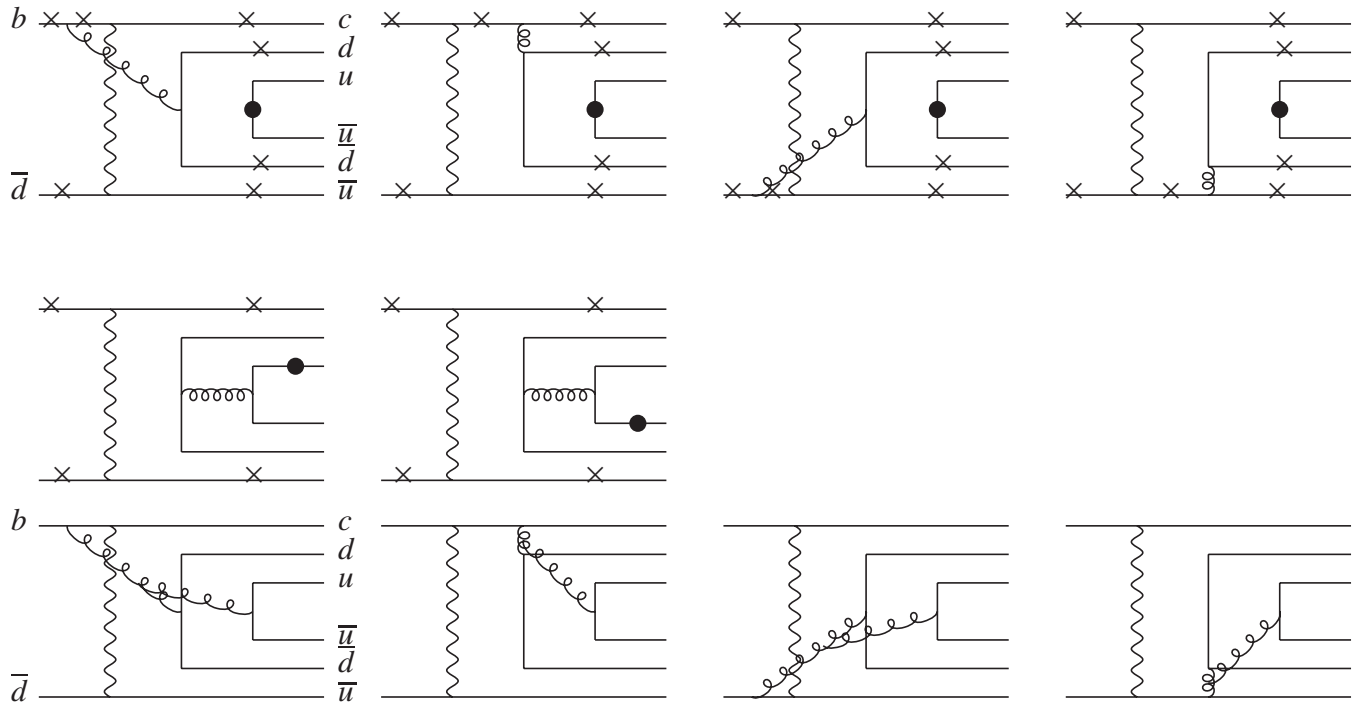

FIG. 4. The W exchange diagrams for the $\bar{B}^0 \to \Lambda_c^+ \bar{p}$ decay.

$$H^{\alpha'\beta'\gamma'\rho'\alpha\beta\gamma\rho}(x, x', y, b, b', b_q, m_B, m_{\Lambda_c}, \nu) = \exp\left[-8\int_\nu^t \frac{d\bar{\mu}}{\bar{\mu}}\gamma_q(\alpha_s(\bar{\mu}))\right] \times H^{\alpha'\beta'\gamma'\rho'\alpha\beta\gamma\rho}(x, x', y, b, b', b_q, m_B, m_{\Lambda_b}). \quad (16)$$

The form factors are obtained by properly grouping relevant terms according to the definition in Eq. (2). Using Eq. (14) we obtain a generic expression for the form factor corresponding to each diagram as

$$A^i(B^i) = \sum_{j=V,A,T} \frac{1}{128N_c^2\sqrt{2N_c}} f_P f_{\Lambda_c} \int [Dx] \times \int [Db]^i C^i(t^i)\Psi_{\Lambda_c}(x)\Phi_P^j(x')\phi_B(1-y) \times \exp[-S^i]H_F^{ij}\Omega^i, \quad (17)$$

where

$$S^i = \sum_{k=2}^{3} s(\omega, x_k p^+) + \sum_{k=1}^{3} s(\omega', x_k' p'^-) + s(\omega_q, (1-y)q^+) + 3\int_\omega^{t^i} \frac{d\bar{\mu}}{\bar{\mu}}\gamma_q(\alpha_s(\bar{\mu})) + 3\int_{\omega'}^{t^i} \frac{d\bar{\mu}}{\bar{\mu}}\gamma_q(\alpha_s(\bar{\mu})) + 2\int_{\omega_q}^{t^i} \frac{d\bar{\mu}}{\bar{\mu}}\gamma_q(\alpha_s(\bar{\mu})) \quad (18)$$

and A^i and B^i represent the form factors contributed by the ith diagram. C^i is an appropriate combination of the Wilson coefficients. The superscript j labels different Lorentz structures V, A, and T of antiproton according to Eq. (7). The explicit expressions for some Ω^i are presented in Appendix A and the corresponding functions H_F^{ij} are given in Appendix E. The total form factors are obtained by summing over the contributions of all the diagrams.

III. NUMERICAL RESULTS

We are now ready to evaluate the form factors numerically. In our calculations, we adopt the distribution amplitude Ψ proposed in Refs. [17,19] for the Λ_c,

$$\Psi(x_1, x_2, x_3) = Nx_1x_2x_3 \exp\left[-\frac{m_{\Lambda_c}^2}{2\beta^2 x_1} - \frac{m_q^2}{2\beta^2 x_2} - \frac{m_q^2}{2\beta^2 x_3}\right]. \quad (19)$$

The normalization constant N is fixed by the condition:

$$\int [dx]\Psi(x_1, x_2, x_3) = 1. \quad (20)$$

Since the decay constant f_{Λ_c} is not experimentally determined so far, one has to invoke a theoretical evaluation to fix it. It is assumed that there is a relation between f_{Λ_c} and f_{Λ_c} as $f_{\Lambda_c} = f_{\Lambda_b}\frac{m_{\Lambda_b}}{m_{\Lambda_c}}$ [17]. In terms of the PQCD method f_{Λ_b} is determined by fitting $B(\Lambda_b \to \Lambda_c l\bar{\nu})$ whose central value is 5% measured by the DELPHI Collaboration [22]. In our previous study of $\Lambda_b \to \Lambda\gamma$ [23], we carried out a new determination for f_{Λ_b}. When fitting the data we first truncate the double logarithmic Sudakov factor in such a way that we require the factor $\exp(-s)$ to be smaller than 1 following the prescription of Ref. [24]. It is noted that our numerical value of f_{Λ_b} is different from that obtained in Ref. [17], where $B(\Lambda_b \to \Lambda_c l\bar{\nu})$ was taken to be 2%. We use the newly measured value instead. In concrete computations, we choose the cutoffs as $\omega = 1.14\min(1/\tilde{b}_1, 1/\tilde{b}_2, 1/\tilde{b}_3)$ and $\omega' = 1.14\min(1/\tilde{b}_1', 1/\tilde{b}_2', 1/\tilde{b}_3')$. The phenomenological factor 1.14 is adopted according to Ref. [25] to make the whole picture more realistic. Moreover, the values of β and m_q in the heavy baryon wave function need to be fixed. In Refs. [16–18], $\beta = 1$ GeV and $m_q = 0.3$ GeV were used to estimate the decay rates of $\Lambda_b \to \Lambda_c l\bar{\nu}$, $\Lambda_b \to pl\bar{\nu}$, and $\Lambda_b \to \Lambda J/\psi$. It is commonly expected that β should not be too much smaller than 1 GeV if the form factors are dominated by the perturbative contributions. To see how different values of β and m_q affect the results, we will let both β and m_q vary within ranges of $0.6 \sim 1.2$ GeV and $0.2 \sim 0.3$ GeV, respectively. Using the fitted value of f_{Λ_b} obtained in Ref. [23], and the relation $f_{\Lambda_c} = f_{\Lambda_b}\frac{m_{\Lambda_b}}{m_{\Lambda_c}}$, we listed f_{Λ_c} in Table II for different parameter sets.

The proton distribution amplitudes have been studied using the King-Sachrajda model. In this work, we adopt the model proposed in Ref. [20],

$$\Phi(x_i, \omega) = \phi_{as}(x_1, x_2, x_3)\sum_{j=0}^{5} N_j\left[\frac{\alpha_s(\omega)}{\alpha_s(\mu_0)}\right]^{b_j/(4\beta_0)} \times a_j A_j(x_i),$$
$$\phi_{as}(x_1, x_2, x_3) = 120x_1x_2x_3. \quad (21)$$

with $\mu_0 \approx 1$ GeV; the constants N_j, a_j, b_j and the Appel polynomials A_j are listed in Table III [16].

TABLE II. Decay constant f_{Λ_c} (GeV) for different choices of β and m_q with Sudkov truncation described in the text.

f_{Λ_c}	$\beta = 0.6$ GeV	$\beta = 0.8$ GeV	$\beta = 1$ GeV	$\beta = 1.2$ GeV
$m_q = 0.2$ GeV	1.70×10^{-3}	2.50×10^{-3}	3.51×10^{-3}	4.71×10^{-3}
$m_q = 0.3$ GeV	3.12×10^{-3}	4.07×10^{-3}	5.22×10^{-3}	6.50×10^{-3}

TABLE III. The constants and polynomials in Eq. (21).

j	a_j	N_j	b_j	$A_j(x_i)$
0	1.00	1	0	1
1	0.310	21/2	20/9	$x_1 - x_3$
2	−0.370	7/2	24/9	$2 - 3(x_1 + x_3)$
3	0.630	63/10	32/9	$2 - 7(x_1 + x_3) + 8(x_1^2 + x_3^2) + 4x_1x_3$
4	0.00333	567/2	40/9	$x_1 - x_3 - \frac{4}{3}(x_1^2 - x_3^2)$
5	0.0632	81/5	42/9	$2 - 7(x_1 + x_3) + \frac{14}{3}(x_1^2 + x_3^2) + 14x_1x_3$

TABLE IV. Branching ratio ($\times 10^{-5}$) for different choices of β and m_q with Sudakov truncation described in the text.

BR	$\beta = 0.6$ GeV	$\beta = 0.8$ GeV	$\beta = 1$ GeV	$\beta = 1.2$ GeV
$m_q = 0.2$ GeV	4.6	2.6	3.6	4.2
$m_q = 0.3$ GeV	3.2	5.1	2.3	3.1

The constant f_P is fixed to be [20]

$$f_P(\omega) = f_P(\mu_0)\left[\frac{\alpha_s(\omega)}{\alpha_s(\mu_0)}\right]^{1/(6\beta_0)}, \tag{22}$$

with $f_P(\mu_0) = (5.2 \pm 0.3) \times 10^{-3}$ GeV^2.

The B meson distribution amplitude is given as [21]

$$\phi_B(x,b) = N_B x^2(1-x)^2 \exp\left[-\frac{m_B^2 x^2}{2\omega_b^2} - \frac{1}{2}(\omega_b b)^2\right], \tag{23}$$

where $\omega_b = 0.4$ GeV and $N_B = 91.74$ GeV for $f_B = 0.19$ GeV.

Finally, when obtaining the branching ratio of $\bar{B}^0 \to \Lambda_c^+ \bar{p}$, for definitiveness we fix the rest of the parameters as following. The parameter $\Lambda_{\rm QCD}$ which enters in the strong coupling constant and various Wilson coefficients is set to be $\Lambda_{\rm QCD} = 0.2$ GeV. For the Cabibbo-Kobayashi-Maskawa quark-mixing matrix parameters, we take their central values [6]: $s_{12} = 0.2243$, $s_{23} = 0.0413$, $s_{13} = 0.0037$, and $\delta_{13} = 1.05$. We take two typical values for m_q as 0.2 and 0.3 GeV and let β vary within a reasonable range to carry out the numerical computations.

The theoretical values of the branching ratio for different β and m_q are listed in Table IV. Our numerical results indicate that BR($\bar{B}^0 \to \Lambda_c^+ \bar{p}$) $= (2.3 \sim 5.1) \times 10^{-5}$. We see that the results are consistent with experimental data. With the values $\beta = 1$ GeV and $m_q = 0.3$ GeV used in Refs. [16–18], BR($\bar{B}^0 \to \Lambda_c^+ \bar{p}$) $= 2.3 \times 10^{-5}$.

IV. DISCUSSIONS AND CONCLUSIONS

In this work, we apply the PQCD method to study the branching ratio of $\bar{B}^0 \to \Lambda_c^+ \bar{p}$. The new measurements on the branching ratio by CLEO and Belle indicate that the previous theoretically estimated branching ratio in various phenomenological models are obviously larger than the data, therefore a better treatment is needed. We take the PQCD as an approach instead since it has been successful in dealing with mesonic B decays. As we discussed in the introduction, the PQCD approach should be well applicable in this case, because the momentum match demands the gluons exchanged between quarks to be ''hard'' and the perturbative contributions dominate. Indeed, our numerical result is satisfactorily consistent with the measured value by the Belle Collaboration.

There are model-related parameters in various wave functions which may influence the numerical results. We obtain them by fitting data, thus the theoretical uncertainties would be much reduced. In fact, except the part involving the wave functions of the hadrons, all the calculations are done in the framework of PQCD. As long as the perturbative approach is applicable, the derivations follow the general principles of quantum field theory. Therefore, the model dependence is further reduced.

There is another source of possible uncertainty coming from the prescription of demanding the Sudakov factor $\exp(-s)$ to be less than one as proposed in Ref. [24]. This truncation seems to be just a convenient choice to suppress the amplitude. We therefore have carried out a calculation without the truncation for a comparison. Indeed, we find that in certain kinematic regions, the Sudakov factor is larger than 1. Therefore, without Sudakov truncation the resulting branching ratio is larger, sometimes by a factor of 2. With more accurate data, one can pin down the detailed differences. Since our results show that the predicted branching ratio with Sudakov truncation is close to experimental range, the prescription outlined in Ref. [24] is to be a reasonable way for calculations.

In conclusion, we have calculated the branching ratio of $\bar{B}^0 \to \Lambda_c^+ \bar{p}$ in the PQCD approach. We find that the predicted branching ratio for BR($\bar{B}^0 \to \Lambda_c^+ \bar{p}$) in the PQCD approach can vary over a range of $(2.3 \sim 5.1) \times 10^{-5}$ with the largest uncertainty coming from the parameters in the wave function of Λ_c^+. With the favored values for the

parameters in the Λ_c^+ wave function, $\beta = 1$ GeV and $m_q = 0.3$ GeV, the branching ratio is about 2.3×10^{-5} which is satisfactorily consistent with the value measured by experiments.

ACKNOWLEDGMENTS

We thank Professor Cheng who suggested we investigate this interesting topic for fruitful discussions. This work is supported in part by the NNSC, NSC, and NCTS.

APPENDIX A: THE b MEASURES

Here and in the following appendices, we provide some details about the calculations. We will show some details for diagrams Fig. 1 (a1), Fig. 2 (b2), and Fig. 3 (c1) which represent each of the three categories Figs. 1–3.

The ordinary b measure is defined as

$$[d\mathbf{b}] = \frac{d^2\mathbf{b}}{(2\pi)^2}. \tag{A1}$$

The explicit forms of $[D\mathbf{b}]^i$ for diagrams Fig. 1 (a1), Fig. 2 (b2), and Fig. 3 (c1) are given by

$$\begin{aligned}
[D\mathbf{b}]^{(a1)} &= [d\mathbf{b}_2][d\mathbf{b}_3'][d\mathbf{b}_q], \\
[D\mathbf{b}]^{(b2)} &= [d\mathbf{b}_2][d\mathbf{b}_1'][d\mathbf{b}_q], \\
[D\mathbf{b}]^{(c1)} &= [d\mathbf{b}_2][d\mathbf{b}_1'][d\mathbf{b}_2'][d\mathbf{b}_q].
\end{aligned} \tag{A2}$$

APPENDIX B: HARD SCATTERING AMPLITUDES $H^{i,\alpha'\beta'\gamma'\rho'\alpha\beta\gamma\rho}(x_i, x_i', y, \mathbf{k}_T, \mathbf{k}_T', \mathbf{q}_T, m_B, m_{\Lambda_c})$

Expressions of amplitude $H^{i,\alpha'\beta'\gamma'\rho'\alpha\beta\gamma\rho}(x_i, x_i', y, \mathbf{k}_T, \mathbf{k}_T', \mathbf{q}_T, m_B, m_{\Lambda_c})$ for diagram Fig. 1 (a1) There is only one Lorentz structure for the γ matrix in the effective Hamiltonian, $O_\mu = \gamma_\mu L$.

For the hard amplitude of Fig. 1 (a1):

$$\begin{aligned}
&H^{a1,\alpha'\beta'\gamma'\rho'\alpha\beta\gamma\rho}(x_i, x_i', y, \mathbf{k}_T, \mathbf{k}_T', \mathbf{q}_T, m_B, m_{\Lambda_c}) \\
&\quad = [\varepsilon^{abc}\varepsilon^{a'b'c'}(C_1(T^j)_{bb'}(T^iT^jT^i)_{ac'}\delta_{a'c} + C_2(T^j)_{bb'}(T^iT^jT^i)_{cc'}\delta_{aa'})]g_s^4 \\
&\quad\quad \times \frac{(\gamma_\lambda)_{\rho'\gamma'}(\gamma_\theta)_{\beta\beta'}[O_\mu(\not p - \not k_2 + \not k_2' + m_b)\gamma^\lambda(\not q_1 - \not k_2 - \not k_2')\gamma^\theta]_{\gamma\rho}(O^\mu)_{\alpha\alpha'}}{(k_2 + k_2')^2(q_2 - k_3')^2[(q_1 - k_2 - k_2')^2 - m_b^2][(p - k_2 + k_1')^2 - m_b^2]} \\
&\quad = \frac{C_N^{a1} g_s^4(\gamma_\lambda)_{\rho'\gamma'}(\gamma_\theta)_{\beta\beta'}[O_\mu(\not p - \not k_2 + \not k_1' + m_b)\gamma^\lambda(\not q_1 - \not k_2 - \not k_2')\gamma^\theta]_{\gamma\rho}(O^\mu)_{\alpha\alpha'}}{[A_{a1} + (\mathbf{k}_{2T} + \mathbf{k}_{2T}')^2][B_{a1} + (\mathbf{q}_T + \mathbf{k}_{3T}')^2][C_{a1} + (-\mathbf{q}_T + \mathbf{k}_{2T} + \mathbf{k}_{2T}')^2][D_{a1} + (\mathbf{k}_{2T} + \mathbf{k}_{2T}' + \mathbf{k}_{3T}')^2]}
\end{aligned} \tag{B1}$$

with

$$\begin{aligned}
A_{a1} &= (r^2 - 1)x_2x_2'm_B^2, \\
B_{a1} &= (r^2 - 1)x_3'(y - 1)m_B^2, \\
C_{a1} &= m_b^2 + ((r^2 - 1)x_2' + 1)(x_2 - y)m_B^2, \\
D_{a1} &= m_b^2 - (r^2(x_1' - 1) - x_1')(x_2 - 1)m_B^2
\end{aligned} \tag{B2}$$

and the color factor

$$\begin{aligned}
C_N^{a1} &= \varepsilon^{abc}\varepsilon^{a'b'c'}(C_1(T^j)_{bb'}(T^iT^jT^i)_{ac'}\delta_{a'c} \\
&\quad + C_2(T^j)_{bb'}(T^iT^jT^i)_{cc'}\delta_{aa'}) \\
&= -\frac{2}{3}C_1 + \frac{2}{3}C_2.
\end{aligned} \tag{B3}$$

For the hard amplitude of Fig. 2 (b2):

$$\begin{aligned}
&H^{b2,\alpha'\beta'\gamma'\rho'\alpha\beta\gamma\rho}(x_i, x_i', y, \mathbf{k}_T, \mathbf{k}_T', \mathbf{q}_T, m_B, m_{\Lambda_c}) \\
&\quad = \frac{C_N^{b2} g_s^4(\gamma_\lambda(-\not p' - \not k_2 + \not k_1')\gamma_\theta)_{\rho'\gamma'}(\gamma^\theta)_{\beta\beta'}[O_\mu(\not p - \not k_2 + \not k_1' + m_b)\gamma^\lambda]_{\gamma\rho}(O^\mu)_{\alpha\alpha'}}{[A_{b2} + (\mathbf{k}_{2T} + \mathbf{k}_{2T}')^2][B_{b2} + (\mathbf{q}_T + \mathbf{k}_{2T} - \mathbf{k}_{1T}')^2][C_{b2} + (\mathbf{k}_{2T} - \mathbf{k}_{1T}')^2][D_{b2} + (\mathbf{k}_{2T} - \mathbf{k}_{1T}')^2]}
\end{aligned} \tag{B4}$$

with

$$\begin{aligned}
A_{b2} &= x_2x_2'(r^2 - 1)m_B^2, \\
B_{b2} &= x_2(-(x_1' - 1)r^2 + x_1' - y)m_B^2, \\
C_{b2} &= -x_2(r^2 - 1)(x_1' - 1)m_B^2, \\
D_{b2} &= m_b^2 - (x_2 - 1)(r^2(x_1' - 1) - x_1')m_B^2
\end{aligned} \tag{B5}$$

and the color factor

$$\begin{aligned}
C_N^{b2} &= \varepsilon^{abc}\varepsilon^{a'b'c'}(C_1(T^j)_{bb'}(T^iT^iT^j)_{ac'}\delta_{ca'} \\
&\quad + C_2(T^j)_{bb'}(T^iT^iT^j)_{cc'}\delta_{aa'}) \\
&= \frac{16}{3}C_1 - \frac{16}{3}C_2.
\end{aligned} \tag{B6}$$

For the hard amplitude of Fig. 3 (c1):

$$
\begin{aligned}
&H^{c1,\alpha'\beta'\gamma'\rho'\alpha\beta\gamma\rho}(x_i, x_i', y, \mathbf{k}_T, \mathbf{k}_T', \mathbf{q}_T, m_B, m_{\Lambda_c}) \\
&\quad = i[\varepsilon^{abc}\varepsilon^{a'b'c'}f_{jil}(C_1(T^jT^i)_{ac'}(T^l)_{bb'}\delta_{ca'} + C_2(T^jT^i)_{cc'}(T^l)_{bb'}\delta_{aa'})]g_s^4 \\
&\qquad \times \frac{(\gamma_\lambda)_{\rho'\gamma'}(\gamma_\eta)_{\beta\beta'}[O_\mu(\not{p} - \not{k}_2 - \not{k}_1' + m_b)\gamma_\theta]_{\gamma\rho}(O^\mu)_{\alpha\alpha'}}{(k_2 + k_2')^2(-q_2 + k_3')^2(p - q_1 - k_2 - k_1')^2[(p - k_2 - k_1')^2 - m_b^2]}[g^{\theta\lambda}(p - q_1 - k_2 - k_1' \\
&\qquad - (-q_2 + k_3'))^\eta + g^{\lambda\eta}(-q_2 + k_3' - (k_2 + k_2'))^\theta + g^{\eta\theta}(k_2 + k_2' - (p - k_2 - k_1'))^\lambda] \\
&\quad = \frac{iC_N^{c1}g_s^4(\gamma_\lambda)_{\rho'\gamma'}(\gamma_\eta)_{\beta\beta'}[O_\mu(\not{p} - \not{k}_2 - \not{k}_1' + m_b)\gamma_\theta]_{\gamma\rho}(O^\mu)_{\alpha\alpha'}}{[A_{c1} + (\mathbf{k}_{2T}' + \mathbf{k}_{2T}')^2][B_{c1} + (\mathbf{k}_{3T}' + \mathbf{q}_T)^2][C_{c1} + (\mathbf{k}_{2T} + \mathbf{k}_{1T}' + \mathbf{q}_T)^2][D_{c1} + (\mathbf{k}_{2T} + \mathbf{k}_{1T}')^2]} \\
&\qquad \times [g^{\theta\lambda}(p - q_1 - k_2 - k_1' - (-q_2 + k_3'))^\eta + g^{\lambda\eta}(-q_2 + k_3' - (k_2 + k_2'))^\theta \\
&\qquad + g^{\eta\theta}(k_2 + k_2' - (p - k_2 - k_1'))^\lambda]
\end{aligned}
\tag{B7}
$$

with

$$
\begin{aligned}
A_{c1} = x_2x_2'(r^2 - 1)m_B^2, \qquad B_{c1} = (r^2 - 1)x_3'(y - 1)m_B^2 \qquad C_{c1} = (r^2 - 1)(x_2 + y - 1)(x_1' + 1)m_B^2, \\
D_{c1} = m_b^2 + (r^2(x_1' + 1) - x_1')(x_2 - 1)m_B^2,
\end{aligned}
\tag{B8}
$$

and the color factor

$$
\begin{aligned}
C_N^{c1} &= \varepsilon^{abc}\varepsilon^{a'b'c'}f_{jil}(C_1(T^jT^i)_{ac'}(T^l)_{bb'}\delta_{ca'} + C_2(T^jT^i)_{cc'}(T^l)_{bb'}\delta_{aa'}) \\
&= 6iC_1 - 6iC_2.
\end{aligned}
\tag{B9}
$$

APPENDIX C: THE MAXIMAL ONE OF $t_{1,2}$

The maximal one of the hard scales t_1^i and t_2^i for diagrams Fig. 1 (a1), Fig. 2 (b2), and Fig. 3 (c1) are given below:

$$
\begin{aligned}
t_1^{a1} &= \max\left\{\sqrt{|A_{a1}|}, \frac{1}{|\mathbf{b_2} - \mathbf{b_3'} + \mathbf{b_q}|}, \omega, \omega'\right\}, \qquad t_2^{a1} = \max\left\{\sqrt{|B_{a1}|}, \frac{1}{|\mathbf{b_3'}|}, \omega, \omega'\right\} \\
t_1^{b2} &= \max\left\{\sqrt{|A_{b2}|}, \frac{1}{|\mathbf{b_2} + \mathbf{b_1'}|}, \omega, \omega'\right\}, \qquad t_2^{b2} = \max\left\{\sqrt{|B_{b2}|}, \frac{1}{|\mathbf{b_q}|}, \omega, \omega'\right\} \\
t_1^{c1} &= \max\left\{\sqrt{|A_{c1}|}, \frac{2}{|\mathbf{b_2} - \mathbf{b_1'} + \mathbf{b_2'}|}, \omega, \omega'\right\}, \qquad t_2^{c1} = \max\left\{\sqrt{|B_{c1}|}, \frac{2}{|\mathbf{b_2} - \mathbf{b_1'} - \mathbf{b_2'}|}, \omega, \omega'\right\}, \\
t_3^{c1} &= \max\left\{\sqrt{|C_{c1}|}, \frac{2}{|\mathbf{b_2} - \mathbf{b_1'} - 2\mathbf{b_q} - \mathbf{b_2'}|}, \omega, \omega'\right\}
\end{aligned}
$$

APPENDIX D: THE HARD SCATTERING AMPLITUDE

The expressions for the hard scattering amplitude in b and b' space are obtained by making a Fourier transformation on k_T and k_T' space. In the following we given one example for Fig. 1 (a1) as an illustration. We note that the k_T and k_T' dependencies are all in the denominators in the above expressions, one then just needs to consider that part of the Fourier transformation. For Fig. 1 (a1), it is given by

$$
\begin{aligned}
&\Omega^{(a1)}(x_i, x_i', y, \mathbf{k}_T, \mathbf{k}_T', \mathbf{q}_T, m_B, m_{\Lambda_c}) \\
&\quad = \frac{1}{[A_{a1} + (\mathbf{k}_{2T} + \mathbf{k}_{2T}')^2][B_{a1} + (\mathbf{q}_T + \mathbf{k}_{3T}')^2][C_{a1} + (-\mathbf{q}_T + \mathbf{k}_{2T} + \mathbf{k}_{2T}')^2][D_{a1} + (\mathbf{k}_{2T} + \mathbf{k}_{2T}' + \mathbf{k}_{3T}')^2]}.
\end{aligned}
\tag{D1}
$$

The fourier transformed expression is then given by

$$
\begin{aligned}
\Omega^{(a1)}(x_i, x_i', y, b_i, b_i', b_q, m_B, m_{\Lambda_c}) = \int e^{-i(\mathbf{k}_{2T}\cdot\mathbf{b}_2 + \mathbf{k}_{2T}'\cdot\mathbf{b}_2' + \mathbf{k}_{3T}'\cdot\mathbf{b}_3' + \mathbf{q}_T\cdot\mathbf{b}_q)}\Omega^{(a1)}(x_i, x_i', y, \mathbf{k}_T, \mathbf{k}_T', \mathbf{q}_T, m_B, m_{\Lambda_c}) \\
\times d^2\mathbf{k}_{2T}d^2\mathbf{k}_{2T}'d^2\mathbf{k}_{3T}'d^2\mathbf{q}_T.
\end{aligned}
\tag{D2}
$$

Defining $\mathbf{k}_{AT} \equiv \mathbf{k}_{2T} + \mathbf{k}'_{2T}$, $\mathbf{k}_{BT} \equiv \mathbf{q}_T + \mathbf{k}'_{3T}$, $\mathbf{k}_{CT} \equiv -\mathbf{q}_T + \mathbf{k}_{2T} + \mathbf{k}'_{2T}$, and $\mathbf{k}_{DT} \equiv \mathbf{k}_{2T}$, we rewrite the transformation as

$$\begin{aligned}\Omega^{(a1)}(x_i, x'_i, y, b_i, b'_i, b_q, m_B, m_{\Lambda_c}) &= \int \frac{e^{-i[\mathbf{k}_{AT}\cdot(\mathbf{b}'_2-\mathbf{b}'_3+\mathbf{b}_q)+\mathbf{k}_{BT}\cdot\mathbf{b}'_3+\mathbf{k}_{CT}\cdot(\mathbf{b}'_3-\mathbf{b}_q)+\mathbf{k}_{DT}\cdot(\mathbf{b}_2-\mathbf{b}'_2)]}}{(\mathbf{k}^2_{AT}+A_{a1})(\mathbf{k}^2_{BT}+B_{a1})(\mathbf{k}^2_{CT}+C_{a1})((\mathbf{k}_{BT}+\mathbf{k}_{CT})^2+D_{a1})} d^2\mathbf{k}_{AT} d^2\mathbf{k}_{BT} d^2\mathbf{k}_{CT} d^2\mathbf{k}_{DT} \\ &= \int_0^1 \frac{dz_1 dz_2}{z_1(1-z_1)} \frac{\sqrt{X_2}}{\sqrt{|Z_2|}} \Big[\pi^2 K_1\Big(\sqrt{X_2 Z_2}\Big)\theta(Z_2) + \frac{\pi^3}{2}\Big[N_1\Big(\sqrt{X_2|Z_2|}\Big) - iJ_1\Big(\sqrt{X_2|Z_2|}\Big)\Big]\theta(-Z_2)\Big] \\ &\quad \times \Big[2\pi K_0\Big(\sqrt{A_{a1}}|\mathbf{b_2}-\mathbf{b'_3}+\mathbf{b_q}|\Big)\theta(A_{a1}) + \pi^2\Big[-N_0\Big(\sqrt{|A_{a1}|}|\mathbf{b_2}-\mathbf{b'_3}+\mathbf{b_q}|\Big) \\ &\quad + iJ_0\Big(\sqrt{|A_{a1}|}|\mathbf{b_2}-\mathbf{b'_3}+\mathbf{b_q}|\Big)\Big]\theta(-A_{a1})\Big], \end{aligned} \tag{D3}$$

where

$$Z_2 = B_{a1}(1-z_2) + \frac{z_2}{z_1(1-z_1)}[C_{a1}(1-z_1) + D_{a1}z_1] \qquad X_2 = [\mathbf{b'_3} - z_1(\mathbf{b'_3}-\mathbf{b_q})]^2 + \frac{z_1(1-z_1)}{z_2}(\mathbf{b'_3}-\mathbf{b_q})^2. \tag{D4}$$

In the above we have used

$$\begin{aligned}\int d^2k \frac{e^{i\mathbf{k}\cdot\mathbf{b}}}{k^2+A} &= 2\pi K_0\Big(\sqrt{A}|\mathbf{b}|\Big)\theta(A) + \pi^2\Big[-N_0\Big(\sqrt{|A|}|\mathbf{b}|\Big) + iJ_0\Big(\sqrt{|A|}|\mathbf{b}|\Big)\Big]\theta(-A), \\ \int d^2k_1 d^2k_2 \frac{e^{i(\mathbf{k_1}\cdot\mathbf{b_1}+\mathbf{k_2}\cdot\mathbf{b_2})}}{(k_1^2+A)(k_2^2+B)[(k_1+k_2)^2+C]} &= \int_0^1 \frac{dz_1 dz_2}{z_1(1-z_1)} \frac{\sqrt{X_2}}{\sqrt{|Z_2|}}\Big[\pi^2 K_1\Big(\sqrt{X_2 Z_2}\Big)\theta(Z_2) \\ &\quad + \frac{\pi^3}{2}\Big[N_1\Big(\sqrt{X_2|Z_2|}\Big) - iJ_1\Big(\sqrt{X_2|Z_2|}\Big)\Big]\theta(-Z_2)\Big], \end{aligned} \tag{D5}$$

and

$$Z_2 = A(1-z_2) + \frac{z_2}{z_1(1-z_1)}[B(1-z_1) + Cz_1], \qquad X_2 = (\mathbf{b}_1 - z_1\mathbf{b}_2)^2 + \frac{z_1(1-z_1)}{z_2}\mathbf{b}_2^2, \tag{D6}$$

where K_0, K_1, N_0, N_1, J_0, and J_1 are Bessel functions and $\theta(x)$ is aθ function.

In carrying out the Fourier transformations for the other diagrams, two other forms of functions will be encountered. We list them in the following:

$$\int d^2k \frac{e^{i\mathbf{k}\cdot\mathbf{b}}}{(k^2+A)(k^2+B)} = \int_0^1 dz \frac{|\mathbf{b}|}{\sqrt{|Z_1|}}\Big[\pi K_1\Big(\sqrt{Z_1}|\mathbf{b}|\Big)\theta(Z_1) + \frac{\pi^2}{2}\Big[N_1\Big(\sqrt{|Z_1|}|\mathbf{b}|\Big) - iJ_1\Big(\sqrt{|Z_1|}|\mathbf{b}|\Big)\Big]\theta(-Z_1)\Big], \tag{D7}$$

and

$$Z_1 = Az + B(1-z). \tag{D8}$$

The expression of Ω^i for diagrams Fig. 2 (b2) and Fig. 3 (c1) are as follows.

$$\begin{aligned}\Omega^{b2} &= \int_0^1 dz \frac{|\mathbf{b'_1}+\mathbf{b_q}|}{\sqrt{|Z_1|}}\Big[\pi K_1\Big(\sqrt{Z_1}|\mathbf{b'_1}+\mathbf{b_q}|\Big)\theta(Z_1) + \frac{\pi^2}{2}\Big[N_1\Big(\sqrt{|Z_1|}|\mathbf{b'_1}+\mathbf{b_q}|\Big) - iJ_1\Big(\sqrt{|Z_1|}|\mathbf{b'_1}+\mathbf{b_q}|\Big)\Big]\theta(-Z_1)\Big] \\ &\quad \times \Big[2\pi K_0\Big(\sqrt{A_{b2}}|\mathbf{b_2}+\mathbf{b'_1}|\Big)\theta(A_{b2}) + \pi^2\Big(-N_0\Big(\sqrt{|A_{b2}|}|\mathbf{b_2}+\mathbf{b'_1}|\Big) + iJ_0\Big(\sqrt{|A_{b2}|}|\mathbf{b_2}+\mathbf{b'_1}|\Big)\Big)\theta(-A_{b2})\Big] \\ &\quad \times \Big[2\pi K_0\Big(\sqrt{B_{b2}}|\mathbf{b_q}|\Big)\theta(B_{b2}) + \pi^2\Big(-N_0\Big(\sqrt{|B_{b2}|}|\mathbf{b_q}|\Big) + iJ_0\Big(\sqrt{|B_{b2}|}|\mathbf{b_q}|\Big)\Big)\theta(-B_{b2})\Big], \end{aligned} \tag{D9}$$

with

$$Z_1 = C_{b2}z + D_{b2}(1-z). \tag{D10}$$

$$\Omega^{c1} = \frac{1}{2}\Big[2\pi K_0\Big(\sqrt{A_{c1}}\frac{1}{2}|\mathbf{b_2} - \mathbf{b_1'} + \mathbf{b_2'}|\Big)\theta(A_{c1}) + \pi^2\Big(-N_0\Big(\sqrt{|A_{c1}|}\frac{1}{2}|\mathbf{b_2} - \mathbf{b_1'} + \mathbf{b_2'}|\Big) + iJ_0\Big(\sqrt{|A_{c1}|}\frac{1}{2}|\mathbf{b_2} - \mathbf{b_1'} + \mathbf{b_2'}|\Big)\Big)\theta(-A_{c1})\Big]\Big[2\pi K_0\Big(\sqrt{B_{c1}}\frac{1}{2}|\mathbf{b_2} - \mathbf{b_1'} - \mathbf{b_2'}|\Big)\theta(B_{c1}) + \pi^2\Big(-N_0\Big(\sqrt{|B_{c1}|}\frac{1}{2}|\mathbf{b_2} - \mathbf{b_1'} - \mathbf{b_2'}|\Big) + iJ_0\Big(\sqrt{|B_{c1}|}\frac{1}{2}|\mathbf{b_2} - \mathbf{b_1'} - \mathbf{b_2'}|\Big)\Big)\theta(-B_{c1})\Big]\Big[2\pi K_0\Big(\sqrt{C_{c1}}\frac{1}{2}|-\mathbf{b_2} + \mathbf{b_1'} + \mathbf{b_2'} + 2\mathbf{b_q}|\Big)\theta(C_{c1}) + \pi^2\Big(-N_0\Big(\sqrt{|C_{c1}|}\frac{1}{2}|-\mathbf{b_2} + \mathbf{b_1'} + \mathbf{b_2'} + 2\mathbf{b_q}|\Big) + iJ_0\Big(\sqrt{|C_{c1}|}\frac{1}{2}|-\mathbf{b_2} + \mathbf{b_1'} + \mathbf{b_2'} + 2\mathbf{b_q}|\Big)\Big)\theta(-C_{c1})\Big]\Big[2\pi K_0\Big(\sqrt{D_{c1}}|\mathbf{b_2} - \mathbf{b_2'} - \mathbf{b_q}|\Big)\theta(D_{c1}) + \pi^2\Big(-N_0\Big(\sqrt{|D_{c1}|}|\mathbf{b_2} - \mathbf{b_2'} - \mathbf{b_q}|\Big) + iJ_0\Big(\sqrt{|D_{c1}|}|\mathbf{b_2} - \mathbf{b_2'} - \mathbf{b_q}|\Big)\Big)\theta(-D_{c1})\Big]. \tag{D11}$$

APPENDIX E: EXPRESSIONS FOR H_F^{ij}

H_F^{ij} corresponds to the form factors defined in Eq. (2) with a ''tilde'' for $\bar{B}^0 \to \Lambda_c^+ \bar{p}$. The expressions for diagrams Fig. 1 (a1), Fig. 2 (b2), and Fig. 3 (c1) are listed in the following.

For the hard amplitudes of Fig. 1 (a1):

$$\tilde{A}^V = \tilde{A}^A = \tilde{B}^V = \tilde{B}^A = 16m_B^5 r^2(-1 + r^2)(1 - y), \qquad \tilde{A}^T = -\tilde{B}^T = 32m_B^5 r^2(-1 + r^2)(1 - y). \tag{E1}$$

For the hard amplitudes of Fig. 2 (b2):

$$\tilde{A}^V = -\tilde{A}^A = -\tilde{B}^V = \tilde{B}^A = -16m_B^5 r(-1 + r^2)x_2^2. \tag{E2}$$

For the hard amplitudes of Fig. 3 (c1):

$$\begin{aligned}
\tilde{A}^V &= \tilde{B}^A = 8m_B^5 r(1 - r^2)(1 + x_2 - y - r(-2 + x_2 + 2y) - (-1 + x_2)(x_2' - x_3' + r^2(-x_2' + x_3') + r(-2 + x_2 + 2y))),\\
\tilde{A}^A &= \tilde{B}^V = -8m_B^5 r(1 - r^2)(1 + x_2 - y + r(-2 + x_2 + 2y) + (-1 + x_2)(-x_2' + r^2(x_2' - x_3') + x_3' + r(-2 + x_2 + 2y))),\\
\tilde{A}^T &= -\tilde{B}^T = 16m_B^5 r^2(-1 + r^2)x_2(-2 + x_2 + 2y).
\end{aligned} \tag{E3}$$

[1] H. Albrecht (ARGUS Collaboration), Phys. Lett. B **209**, 119 (1988).

[2] B. Aubert *et al.* (*BABAR* Collaboration), Phys. Rev. D **69**, 091503 (2004); Phys. Rev. D **72**, 051101 (2005); Phys. Rev. Lett. **90**, 231801 (2003); M. C. Chang *et al.* (Belle Collaboration), Phys. Rev. D **71**, 072007 (2005); Q. L. Xie *et al.*, Phys. Rev. D **72**, 051105 (2005); M. Z. Wang *et al.*, Phys. Rev. Lett. **90**, 201802 (2003); **92**, 131801 (2004); Y. J. Lee *et al.*, Phys. Rev. Lett. **93**, 211801 (2004); M. Z. Wang *et al.*, Phys. Lett. B **617**, 141 (2005); K. Abe *et al.*, Phys. Rev. Lett. **88**, 181803 (2002); A. Bornheim *et al.* (CLEO Collaborqtion), Phys. Rev. D **68**, 052002 (2003); T. E. Coan *et al.*, *ibid.* **59**, 111101 (1999); S. Anderson *et al.*, Phys. Rev. Lett. **86**, 2732 (2001).

[3] N. Gabyshev *et al.* (Belle Collaboration), hep-ex/0409005; Phys. Rev. Lett. **90**, 121802 (2003); R. Chistov *et al.* (Belle Collaboration), Phys. Rev. D **74**, 111105 (2006).

[4] B. Aubert *et al.* (*BABAR* Collaboration), hep-ex/0607055; T. Berger-Hryn'ova, Ph.D. thesis, SLAC [SLAC Report No. SLAC-R-810].

[5] S. A. Dytman *et al.* (CLEO Collaboration), Phys. Rev. D **66**, 091101 (2002).

[6] S. Eidelman *et al.* (Particle Data Group), Phys. Lett. B **592**, 1 (2004).

[7] Yong-Yeon Keum and Hsiang-nan Li, Phys. Rev. D **63**, 074006 (2001); Chuan-Hung Chen, Yong-Yeon Keum, and Hsiang-nan Li, Phys. Rev. D **64**, 112002 (2001); Yong-Yeon Keum, Hsiang-nan Li, and A. I. Sanda, Phys. Rev. D **63**, 054008 (2001); Chuan-Hung Chen, Yong-Yeon Keum, and Hsiang-nan Li, Phys. Rev. D **66**, 054013 (2002); Cai-Dian Lü, Kazumasa Ukai, and Mao-Zhi Yang, Phys. Rev. D **63**, 074009 (2001); Cai-Dian Lü and Mao-Zhi Yang, Eur. Phys. J. C **23**, 275 (2002).

[8] Xia-Gang He, B. McKellar, and D.-D. Wu, Phys. Rev. D

41, 2141 (1990).
[9] V. Chernyak and I. Zhitnitsky, Nucl. Phys. **B345**, 137 (1990).
[10] G. Lu, X. Xue, and J. Liu, Phys. Lett. B **259**, 169 (1991).
[11] M. Jarfi *et al.*, Phys. Rev. D **43**, 1599 (1991); Phys. Lett. B **237**, 513 (1990).
[12] P. Ball and H. G. Dosch, Z. Phys. C **51**, 445 (1991).
[13] H. Y. Cheng and K. C. Yang, Phys. Rev. D **67**, 034008 (2003); **65**, 054028 (2002).
[14] H. Y. Cheng,Int. J. Mod. Phys. A **21**, 4209 (2006).
[15] G. Buchalla, A. J. Buras, and M. E. Lautenbacher, Rev. Mod. Phys. **68**, 1125 (1996).
[16] Hsien-Hung Shih, Shih-Chang Lee, and Hsiang-nan Li, Phys. Rev. D **59**, 094014 (1999).
[17] Hsien-Hung Shih, Shih-Chang Lee, and Hsiang-nan Li, Phys. Rev. D **61**, 114002 (2000).
[18] Chung-Hsien Chou, Hsien-Hung Shih, Shih-Chang Lee, and Hsiang-nan Li, Phys. Rev. D **65**, 074030 (2002).
[19] W. Loinaz and R. Akhoury, Phys. Rev. D **53**, 1416 (1996); F. Schlumpf, Ph.D. thesis, Zurich University, 1992.
[20] V. L. Chernyak, A. A. Ogloblin, and I. R. Zhitnitsky, Z. Phys. C **42**, 569 (1989).
[21] A. G. Grozin and M. Neubert, Phys. Rev. D **55**, 272 (1997); M. Beneke and T. Feldmann, Nucl. Phys. **B592**, 3 (2001); M. Beneke, G. Buchalla, M. Neubert, and C. T. Sachrajda, Nucl. Phys. **B591**, 313 (2000); T. Kurimoto, Hsiang-nan Li, and A. I. Sanda, Phys. Rev. D **65**, 014007 (2001).
[22] J. Abdallah *et al.* (DELPHI Collaboration), Phys. Lett. B **585**, 63 (2004).
[23] Xiao-Gang He, Tong Li, Xue-Qian Li, and Yu-Ming Wang, Phys. Rev. D **74**, 034026 (2006).
[24] Yong-Yeon Keum, T. Kurimoto, Hsiang-nan Li, Cai-Dian Lü, and A. I. Sanda, Phys. Rev. D **69**, 094018 (2004).
[25] Bijoy Kundu, Hsiang-nan Li, Jim Samuelsson, and Pankaj Jain, Eur. Phys. J. C **8**, 637 (1999).